The Influence of Ashing Temperature on Ash Fouling and Slagging Characteristics during Combustion of Biomass Fuels

Xiwen Yao,[a] Kaili Xu,[a,*] Fang Yan,[a] and Yu Liang [b]

Three typical biomass fuels—rice husk, rice straw, and corn cobs—were combusted to understand the effects of ashing temperature on ash fouling and slagging characteristics. The ashes generated from combustion at 600 °C and 815 °C were characterized thoroughly with regard to their chemical composition. The systematic slagging/fouling indices of biomass were used to study the effects of ashing temperature on ash fouling and slagging propensities. The results showed that ashing temperature had a remarkable influence on ash composition, particle size distribution, ash morphology, ash fusibility, and thermal properties. Increased ashing temperature resulted in the expansion of ash particles together with the volatilization of alkali metals in the form of inorganic salts. Morphology analysis indicated that high ashing temperatures promoted biomass ash slagging. Ash fusion points increased at elevated ashing temperatures, while the ash content decreased. As a result of the volatilization and decomposition of biomass ash, a four-step mechanism of weight loss was clearly identified by thermal analysis. All prepared biomass ashes resulted in slagging and fouling problems at different levels during the thermo-chemical conversion of biomass.

Keywords: Biomass fuels; Ashing temperature; Ash properties; Slagging and fouling; Applications

Contact information: a: School of Resources and Civil Engineering and b: College of Information Science and Engineering, Northeastern University, Shenyang 110819, PR China;
** Corresponding author: neu_kailixu@126.com*

INTRODUCTION

As a green renewable energy source, biomass will have increasing importance in the near future. Many countries are emphasizing the exploration of biomass energy; for example, the utilization of available biomass residuals will reach up to 50 million tons in China after 10 years (Xiong *et al*. 2008). Currently, various technologies are used for the thermo-chemical conversion of biomass. The most commonly used technologies include direct combustion, gasification, thermal pyrolysis, liquefaction, and hydrogen production (Brown *et al*. 2000; Demirbas 2002; Loffler *et al*. 2002; Sheth and Babu 2009; Iliuta *et al*. 2010; Sun *et al*. 2010).

The use of waste biomass residuals as renewable fuels generally produces large quantities of biomass ash; without proper disposal, this ash may cause environmental pollution (Umamaheswaran and Batra 2008). These residual ashes after the thermo-chemical conversion of biomass fuels are usually regarded as inorganic mineral materials (Thy *et al*. 2006). Nowadays, due to the renewable, eco-friendly, and availability cost nature for using biomass residuals, as well as lack of competing markets, huge quantities of biomass ash can be generated every day, which requires proper disposal. Meanwhile, commercial utilization of these inorganic materials does not seem to be widely reported;

thus further studying the ash related issues as well as ash properties is worthwhile. In addition, these residual inorganic materials are suggested to be easily melted, volatilized, and bonded with the tar droplets inside the biomass-fired power boilers or other equipment for biomass conversion, resulting in slagging, fouling, and corrosion problems (Wang *et al*. 2008). During the thermo-chemical conversion of biomass, these residual inorganic materials also form slag and fly ash deposits on the heating surface, which deteriorate burning, retard heat transfer, and result in high temperature corrosion and super-heater explosion (Aho and Silvennoinen 2004; Knudsen *et al*. 2004; Szemmelveisz *et al*. 2009; Niu *et al*. 2010a; Niu *et al*. 2010b).

There have been numerous studies on the physicochemical properties of different biomass ashes, such as herbaceous biomass ash (Du *et al*. 2014), bagasse fly ash (Batra *et al*. 2008; Umamaheswaran and Batra 2008), capsicum stalk ash and cotton stalk ash (Niu *et al*. 2010a), seaweed biomass ash (Wang *et al*. 2008), cashew nut ash (Ogundiran *et al*. 2011), wheat hull ash (Terzioglu *et al*. 2013), peanut hull ash (Liao *et al*. 2011), woody biomass ash (Skrifvars *et al*. 2004; Ban and Ramli 2011), sunflower husk ash (Quaranta *et al*. 2011), corn straw ash and bamboo ash (Fang and Jia 2012), *etc*. The physical and chemical properties of different biomass ashes are quite different. Even for the same kind of biomass fuels, the carbon content of their relevant ashes formed under different ashing temperatures also present substantial differences. Within the various studies of biomass ashes, only a few have focused on the agglomeration characteristics during the thermo-chemical conversion process of biomass fuels (Scala and Chirone 2008; Niu *et al*. 2010b; Teixeira *et al*. 2012), and the influences of ashing temperature on the properties of different biomass ashes are still incompletely understood or uncertain in many details, so further investigations are required. Considering the biomass availability, area-specific agriculture residues, and related transportation costs, it is important to explore various local biomasses for their suitability as fuels.

In this paper, three typical and common biomass fuels, namely rice husk (RH), rice straw (RS), and corn cobs (CC), were chosen to examine the influence of ashing temperature on ash fouling and slagging characteristics during the combustion of biomass fuels. To investigate these impacts more accurately as well as provide a reference for evaluating the potential applications of these waste biomass ashes in different industries, a series of qualitative and quantitative analysis methods were performed, including laser particle size analysis, X-ray fluorescence (XRF), scanning electron microscopy (SEM), thermogravimetric analyzer (TGA), differential thermal analyzer (DTA), muffle furnace burning test, ash melting point test system, and the systematic slagging and fouling indexes of biomass fuels. Here, the ash characteristics-related projects mainly involves particle size distribution, chemical composition, morphology, thermal analysis, ash fusion, and transformation properties of the inorganic components in ash. This data revealed the effects of ashing temperature and burning time on the ash agglomeration behavior, which influences the ash slagging and fouling characteristics.

EXPERIMENTAL

Biomass Materials

The biomass samples used to prepare ashes were obtained from the peripheral rural area of Shenyang, Liaoning province, China. Prior to ash preparation, the biomass materials were firstly oven-dried at 105 ± 0.5 °C for 24 h and then smashed *via* a shredder

(TPX2000, Zhangqiu Instruments Co, Ltd., Weifang, China). Secondly, they were further pulverized to be homogenized. Finally, those biomass particles that passed through a 100 mesh sieve (≤ 0.154 mm) were collected in a closed vessel and retained for analysis. Table 1 shows the proximate and ultimate analysis results of these biomass materials. All values presented a reproducibility with the standard deviation of less than 2.0%, and the relative precision of the measurements was 0.5%.

Table 1. Proximate and Ultimate Analysis of Biomass (on Air-dried Basis)

Biomass Materials	Proximate Analysis (wt.%)				Ultimate Analysis (wt.%)				
	Volatile Matter	Moisture	Fixed Carbon	Ash	C	H	O	N	S
RH	70.82	0.79	13.19	15.20	45.93	5.61	31.29	1.03	0.15
RS	72.43	1.38	14.37	11.82	43.89	5.18	36.37	1.25	0.11
CC	79.25	0.87	17.64	2.24	47.26	5.79	43.23	0.56	0.05

Preparation of Biomass Ash

There are no specific standards that are available for preparation of biomass ash in China. The ashing temperatures were respectively set at 600 °C according to ASTM E1755-01 standard (2015) and 815 °C according to GB/T 212 (2008). During the biomass ashing process, the pulverized samples were put in a muffle furnace (SX2-15-12, Shuangyu Instruments Co., Ltd., Jiangsu, China) and kept for 2 h at 600 or 815 °C. The atmosphere in the furnace was free air. The storage interval was 1 °C. The ash samples were stored in an airtight container.

Experimental Apparatus

The particle size distribution of biomass ash was analyzed by laser particle size analyzer (Winner 3001, Jinan Micro-nano Particle Instrument Co. Ltd., Shandong, China) equipped with the He-Ne laser diffraction (λ = 632.8 nm). The chemical composition of the ash was obtained by an X-ray fluorescence spectrometer (XRF) (ZSX100e, Rigaku Co. Ltd., Tokyo, Japan).

The ash morphology was observed by scanning electron microscopy (SEM) (Ultra Plus, Carl Zeiss Co. Ltd., Oberkochen, Germany) with an accelerating voltage of 20 to 30 kV. The ash fusibility was determined using an ash fusion determination meter (5E-AFIII, Kaiyuan Instruments Co, Ltd., Changsha, China).

The effects of ashing temperature and lasting time on the slagging morphology and interior structure of biomass ash were studied through biomass burning tests, which were performed in the muffle furnace.

The thermal properties of biomass ash were obtained by a thermal balance (NETZSCH-STA449 F3, Selb, Germany) to obtain the weight loss information and differential thermal analysis (DTA) to record the phase transition. Additionally, the sensitivity of the thermal balance was 1 μg and 0.01 °C. The biomass samples used for each test were 5 mg.

The heating temperature ranged from 25 to 1200 °C at a heating rate of 20 °C/min. The heating was conducted in dry air, and the flow rate was 30 mL/min. Experiments were carried out at least three times.

RESULTS AND DISCUSSION

Particle Size Distribution

Figure 1 displays the micrographs of homogenized ash powders obtained at 600 and 815 °C. The granularity analysis for these biomass ash samples are summarized in Table 2. The tests were repeated three times, and the average value was used to minimize the error. The medium diameter (D_{50}) of the biomass ash formed at 600 °C was much larger than that of the 815 °C ash, but the specific surface area of 815 °C ash was relatively larger than that of the 600 °C ash.

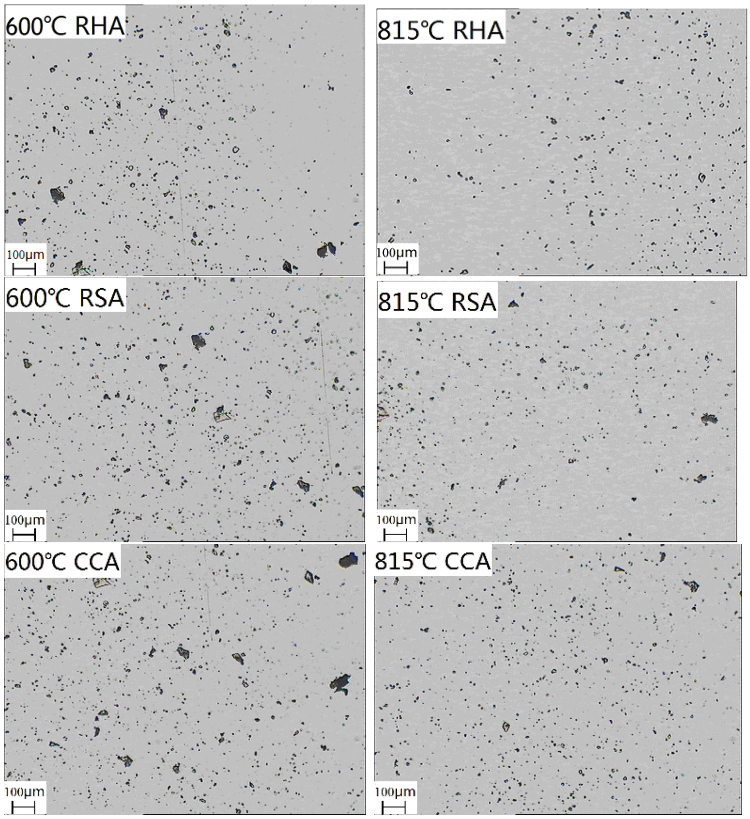

Fig. 1. Particle size distribution of biomass ashes

Table 2. Granularity Analysis of Biomass Ash at Different Ashing Temperatures

Ash samples	D_{10}/μm	D_{25}/μm	D_{50}/μm	D_{75}/μm	D_{90}/μm	Q	L	S (cm^2/g)
600 °C RHA	5.7	9.1	16.0	22.7	26.7	0.825	0.978	2128.762
815 °C RHA	2.6	4.9	9.8	15.1	18.9	0.861	0.872	3868.225
600 °C RSA	5.9	11.7	23.8	36.9	44.6	0.869	0.998	1791.272
815 °C RSA	5.6	8.5	14.9	21.5	25.3	0.803	0.918	2298.352
600 °C CCA	2.1	4.3	14.3	18.4	20.6	0.849	0.863	3915.785
815 °C CCA	2.0	3.5	8.2	19.5	21.7	0.846	0.928	4686.362

D_{10}, ash particle diameter, below which the accumulated percentage is 10%; D_{25}, ash particle diameter, below which the accumulated percentage is 25%, and so on; D_{av}, mean diameter; Q, spherical degree; L, the length-width ratio; S/V, ratio of the total surface area to volume of ash particles.

As shown in Fig. 1, there was a greater quantity of larger particles in the 600 °C ash than in the 815 °C ash, indicating that the particle size of the ashes of biomass fuels decreased remarkably with increasing ashing temperature. The expansion of the trapped volatile matters from the solid biomass substrates during combustion causes the thermal expansion of ash powders; consequently, the severe expansion of ash particles at relatively high temperatures increases the specific surface area. In addition, the values of spherical degree and length-width ratio for the 600 and 815 °C ashes revealed no obvious trends in particle shape with increasing temperature. Thus, ashing temperature had a relatively small influence on the geometrical shapes of ash particles.

Chemical Composition Analysis

The chemical composition results of biomass ashes determined by XRF are presented in Table 3. As a note, the content of chlorine in the ashes was measured by ion chromatograph (IC/792 Basic) using the extraction method according to ASTM/E776-87R04 (2015).

Table 3. Chemical Composition of Biomass Ash Determined by XRF (wt.%)

Sample	SiO_2	K_2O	Na_2O	CaO	MgO	SO_3	P_2O_5	Fe_2O_3	Al_2O_3	Cl
600 °C RHA	94.79	1.86	0.39	0.75	0.55	0.09	0.23	0.86	0.36	0.078
815 °C RHA	95.98	1.72	0.12	0.77	0.43	0.07	0.16	0.35	0.32	0.013
600 °C RSA	73.26	13.46	0.93	4.46	2.14	2.41	1.94	0.49	0.25	0.57
815 °C RSA	77.01	10.83	0.81	4.65	1.67	2.65	1.67	0.31	0.22	0.13
600 °C CCA	31.82	27.55	6.18	5.59	4.81	4.85	2.90	0.83	2.75	12.56
815 °C CCA	34.26	24.09	5.82	6.08	7.43	5.15	3.96	0.65	2.43	9.95

The oxides in biomass ashes can be divided into acidic oxides (SiO_2, Al_2O_3, SO_3, and P_2O_5, *etc*.) and basic oxides (K_2O, CaO, MgO, Na_2O and Fe_2O_3, *etc*.) according to the acidic and basic capacity. These results show that the content of inorganic matter in various biomass ashes at different ashing temperatures is much different; the primary content of the inorganic matter included Si, K, Na, Ca, Mg, Fe, Al, *etc*. Furthermore, the content of alkali metals (such as K and Na) in biomass ashes decreased with increasing temperature, which was mainly attributed to the high volatility of alkali metal during combustion of biomass fuels. In the combustion process, the alkali metals can easily evaporate with increasing temperature in the form of inorganic salts.

The K, Na, and Ca contents in CCA were much higher than those of RHA and RSA, which can be explained by two aspects. After the combustible components of biomass are burned, the release of inorganic matters in different biomass fuels is substantially different during combustion. However, the chemical composition of different biomass fuels is also quite different. Öhman *et al*. (2000) revealed that the alkali metals and their related compounds can form furnace slag or agglomeration samples in the forms of gaseous phases and fly ash particles, which further causes the fouling, slagging, and corrosion problems on the surfaces of thermo-chemical equipment. Additionally, Thompson *et al*. (2003) went into some amount of detail discussing the importance of speciation and ratios of ash species as it pertained to ash slagging by alkali metals. Thus, based on the above analysis, CCA is inferred to be more likely to cause the fouling, slagging, and corrosion because it contained a higher content of alkali metals than RHA and RSA, and the damage on the heat exchanging surface of thermo-chemical equipment caused by CCA could be much greater

than that caused by other ashes.

As shown in Table 2, the content of SiO_2 is predominant in these ashes, especially for RHA, in which the SiO_2 content exceeds more than 94%. There was no obvious variation relationship between the content of SiO_2 and ashing temperature because most of the inert element Si remains in the ashes during the combustion of biomass fuels. Comparison of the chlorine content in the biomass ashes at different ashing temperatures showed that the chlorine content decreased with increasing ashing temperature, which was attributed to the volatility of chlorine at higher temperatures. Wu *et al*. (2013) reported that the release rate of chlorine in the form of gaseous alkali metal chloride rose with the increase of temperature when the temperature exceeded 700 °C.

Morphology Analysis

The SEM photomicrographs of biomass ashes illustrate the surface morphology and fouling/slagging characteristics of biomass ash particles formed at different ashing temperatures. Prior to the morphology analysis of biomass ash samples, a metal spraying treatment (gold/carbon coating for the sake of conductivity) was necessary because the electric conductive performance of biomass ash is poor. After metal spraying treatment, SEM analysis was employed to provide detailed imaging information of biomass ash. Figures 2 through 4 show the SEM images of RHA, RSA, and CCA, respectively.

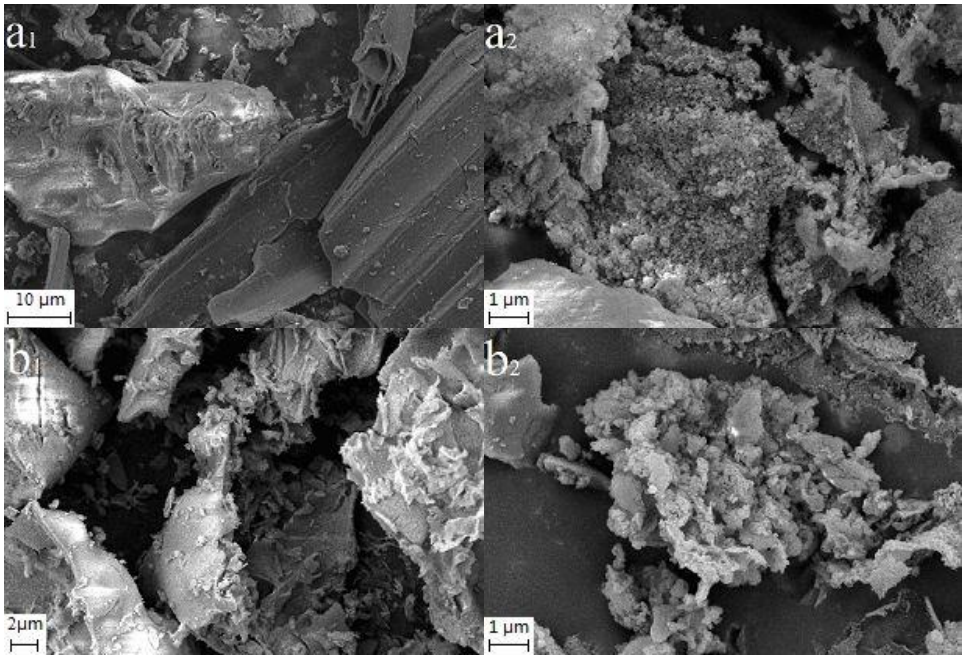

Fig. 2. SEM images of 600 °C RHA (a_1 and a_2) and 815 °C RHA (b_1 and b_2)

As shown in Fig. 2(a1) and Fig. 3(a1), the 600 °C ashes still retained the original structure of interior and exterior of biomass fuels. Figure 2(a1) shows some leaf shape particles in 600 °C RHA, while Fig. 3(a1) exhibits the presence of club-shaped particles, which retained the fibrous characteristics of rice straw feedstock. Figure 2(a2) shows the external surface of 600 °C RHA particles having a loose distribution, while Fig. 3(a2) shows the presence of slight caking in 600 °C RSA. These results illustrate that the RSA is more likely to cause a slagging problem than RHA under the same ashing conditions.

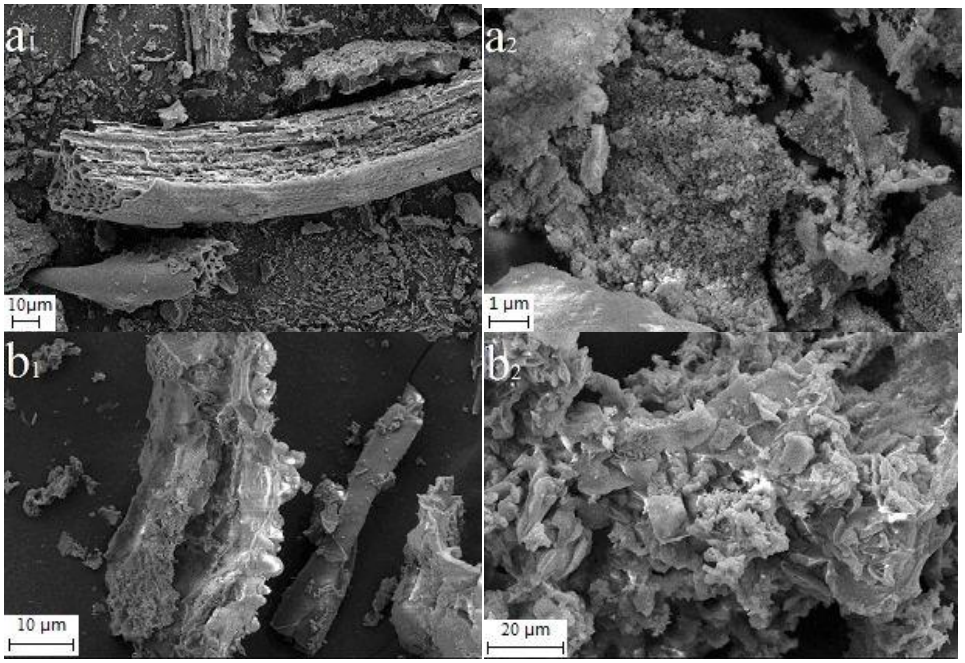

Fig. 3. SEM images of 600 °C RSA (a_1 and a_2) and 815 °C RSA (b_1 and b_2)

Figure 2(b1) shows the floccules attached on the surface of agglomerate, indicating the release of alkali metal compounds in ash. Figure 2(b2) shows a typical agglomerate sample formed at 815 °C, and it appears more compact and rough than 600 °C RHA particles, which had a relatively loose distribution (Fig. 2(a2)). Figure 3(b1) exhibits a piece of cylindrical flake and details of its internal surface. At a higher magnification, the external surface of an agglomerate sample can be clearly seen in Fig. 3(b2).

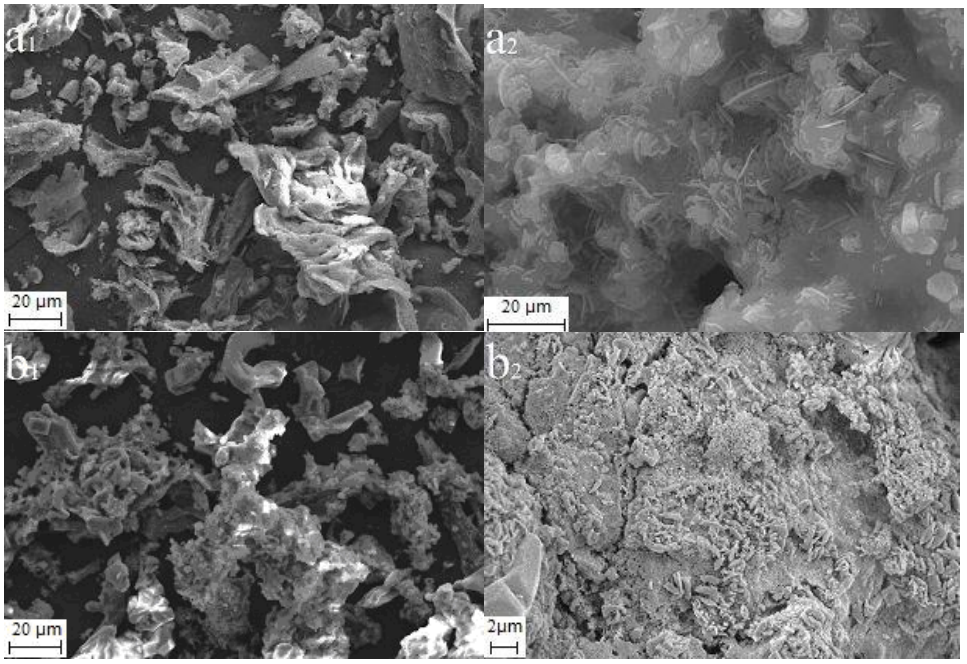

Fig. 4. SEM images of 600 °C CCA (a_1 and a_2) and 815 °C CCA (b_1 and b_2)

Moreover, the contrast of Figs. 2(a1) and (a2) to Figs. 2(b1) and (b2) as well as Figs. 3(a1) and (a2) to Figs. 3(b1) and (b2) suggests that the morphology of biomass ashes was influenced remarkably by ashing temperature, which further indicates that these 600 °C ash particles retained the original skeleton of biomass, while the 815 °C ash particles gradually decomposed with the increment of ashing temperature. This result was mainly attributed to the inadequate burning at the relatively low ashing temperature of 600 °C. Compared with the biomass ashes formed at 600 °C, the amount of ash floccules attached on the surface of agglomerate samples increased with the increment of ashing temperature, which was mainly due to the melting of alkali metal compounds at high temperature. The molten alkali metal compounds can gradually evaporate in the form of gaseous phase and stay on the surface of ash particles (Fang and Jia 2012).

Figure 4(a1) shows the irregularly shaped floccules in 600 °C CCA, which indicates that the slight caking and the ash softening may have begun under 600 °C. Figure 4(a2) exhibits the details of a fused zone of 600 °C CCA. This zone appears to be molten and re-solidified, but, as can be seen in Fig. 4(a2), several partially molten or non-molten ash inclusions were clearly visible in the molten materials. Scala and Chirone (2008) suggested that these ash inclusions are first deposited on the sticky fused surface and then progressively embedded in the molten ash. In previous studies (Yao and Xu 2016; Yao *et al*. 2016), the fused layer was proven to be specifically rich in potassium and chlorine, so it can be inferred that the surface of these molten materials is mostly covered with KCl.

The contrast between Fig. 4(a1) and Fig. 4(b1) reveals that the 815 °C CCA appears more rough and combines more tightly than that of the 600 °C CCA, which indicates that the agglomeration tendency of biomass ash can be aggravated at high temperatures. Figure 4(b2) shows the external surface of a dense agglomerate sample at a higher magnification. The contrast between Fig. 4(a2) and Fig. 4(b2) indicates the important impacts of ashing temperature on the slagging characteristics of biomass ash. The slagging tendency and melting degree of these biomass ashes can be aggravated at relatively high ashing temperatures; at higher temperatures it is more likely for biomass ash to reach low-melting point eutectics on the surface of inert particles in the ash (Scala and Chirone 2008). According to the previous research conducted by Niu *et al*. (2013), the ash fusion characteristics were mainly dependent on the high-temperature molten materials built up by SiO_2, K_3FeO_2, and silicates, which provided a supporting effects of the skeleton-like structure in the ash. Moreover, Niu's other research (Niu *et al*. 2016) suggested that the pure NaCl, KCl, and K_2SO_4 had melting points of 801, 774, and 1069 °C, respectively, but the eutectic temperatures for NaCl - KCl and KCl - K_2SO_4 mixtures could be as low as 657 and 694 °C, respectively, thus further accelerating the slagging tendency and melting degree of biomass ash.

Impacts of Ashing Temperature on Ash Fusion Properties

Ash fusion temperatures were the main factor that restricted the highest technique during the thermo-chemical process. Different ashing temperatures may lead to different pore structure, which affects ash melting temperature, but there has been a lack of studies on the ash fusion points, especially with respect to experimental data and mechanistic analysis. Hence, study of the ash fusion characteristics of the prepared ash samples at different temperatures and on the impacts from ashing temperature (600 and 815 °C) is definitely significant for investigating the fusibility of biomass ashes.

In this work, the pyramid method was used for measuring the biomass ash fusion temperatures according to GB/T 219 (2008), in which a triangular ash cone with a bottom

of 7 mm equilateral triangle and a height of 20 mm was made. The triangle ash cone was heated in free air. The ash samples were heated at 15 to 30 °C/min before 900 °C and 5 to 10 °C/min after 900 °C. In each test, the deformation temperature (DT), softening temperature (ST), hemispherical temperature (HT), and flow temperature (FT) were measured. The ash fusion temperatures of different biomass ashes are shown in Table 4.

Table 4. Fusion Points of Biomass Ash at Different Ashing Temperatures

Ash Samples	DT (°C)	ST (°C)	HT (°C)	FT (°C)
600 °C RHA	1467	1523	1595	>1620
815 °C RHA	1492	1578	1617	>1620
600 °C RSA	998	1176	1238	1314
815 °C RSA	1080	1225	1289	1365
600 °C CCA	862	981	1025	1094
815 °C CCA	910	1013	1063	1176

The DT, ST, HT, and FT of 815 °C ashes were relatively higher than those of 600 °C ashes, indicating the ash fusion points of biomass ash increased with increasing ashing temperature. This result is consistent with previous findings (Xiao *et al*. 2011), which can be explained in two ways.

Firstly, the ash composition analysis in Table 3 showed that the content of alkali metal oxides ($K_2O + Na_2O$) in 600 °C biomass ashes was relatively higher than that of 815 °C biomass ashes. This result indicated that a higher ashing temperature made it easier for alkali metals to volatilize and form the compounds with relatively low melting points, such as chlorides, oxides, and sulfates (Song *et al*. 2003). In contrast, the content of acid metal oxides ($SiO_2 + Al_2O_3$) in 600 °C ashes was a little lower than that of 815 °C ashes. The refractory minerals (such as quartz, kaolinite, and mullite) formed by SiO_2 and Al_2O_3 have high melting points, further increasing the ash fusion points (Wei *et al*. 2014).

Secondly, different ashing temperatures can lead to different pore structures of biomass ash, which remarkably influences the fusion characteristics of biomass ash. Fang and Jia (2012) suggested that the diameter of the pore structure of biomass ash is large when the ashing temperature is relatively high, and those materials with high melting points could play a key role in retaining the stability of the biomass skeleton, resulting in a much higher melting temperature. In other words, when the ashing temperature is relatively lower, more small holes will be present in the pore structure of biomass ash, which can further accelerate the deformation of biomass ash. In addition, the influence of removal of low melting point materials on ash fusion and transformation properties is still uncertain in details. The mechanism resulting in ash deformation and reactions among those inorganic components in the biomass ash also require further study.

Thermal Properties Analysis

The thermogram curves of various biomass ashes as a function of temperature recorded in dry air are shown in Fig. 5. As a note, Figs. 6a through 6f present the TGA-DTA curves of 600 °C RHA, 815 °C RHA, 600 °C RSA, 815 °C RSA, 600 °C CCA, and 815 °C CCA, respectively.

As can be observed in Fig. 5, the thermal decomposition for almost all biomass ashes (except 815 °C RSA (Fig. 5d) and 815 °C CCA (Fig. 5f)) showed stepwise mechanisms, and primarily occurred in the following four steps: less than 200 °C, the evaporation of unbound moisture and the degradation of thermally unstable matters; 200

to 600 °C, oxidation of organic matter; 600 to 800 °C, removal and reaction of inorganic matter; and beyond 800 °C, transformation of residual inorganic matter.

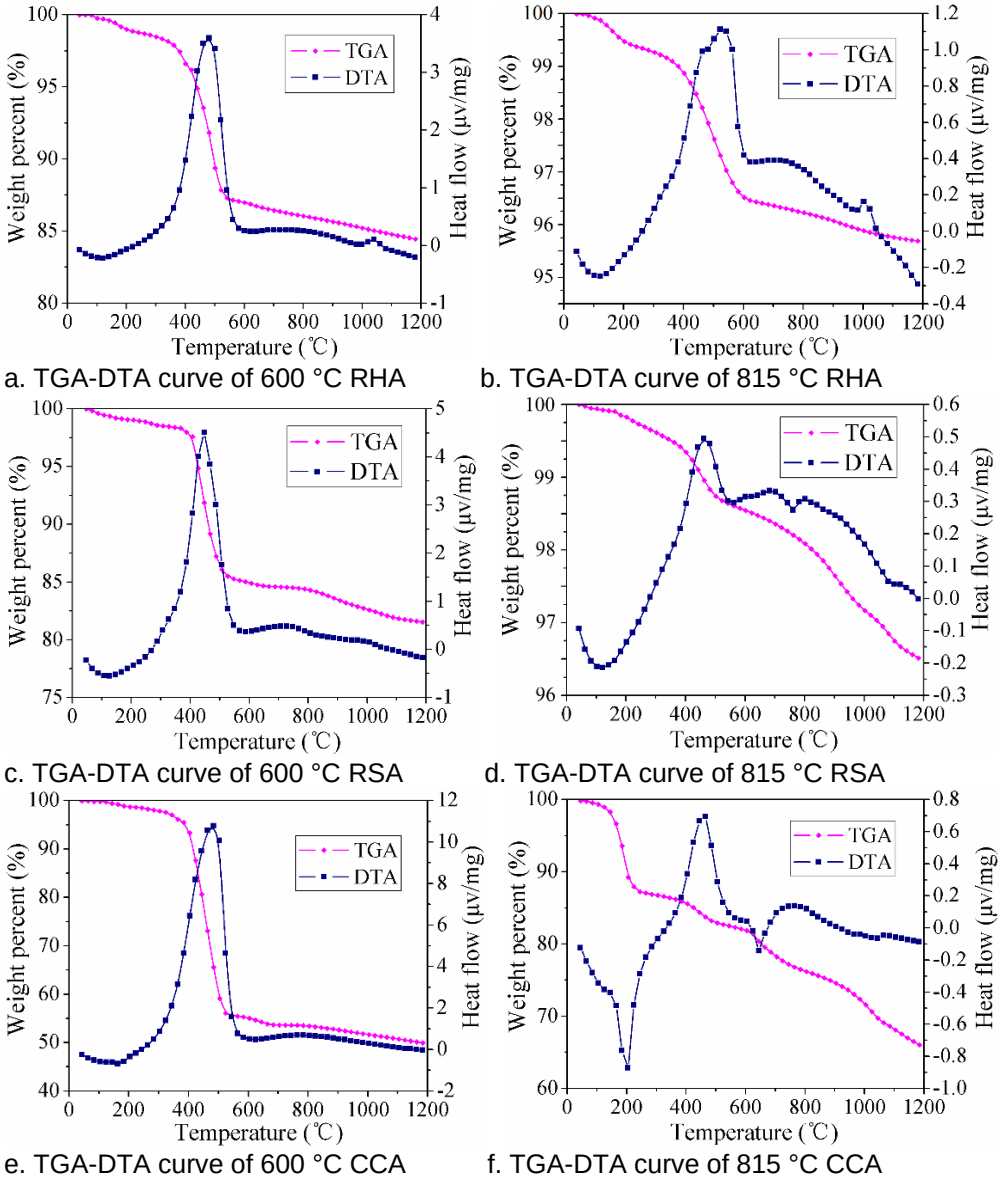

a. TGA-DTA curve of 600 °C RHA
b. TGA-DTA curve of 815 °C RHA
c. TGA-DTA curve of 600 °C RSA
d. TGA-DTA curve of 815 °C RSA
e. TGA-DTA curve of 600 °C CCA
f. TGA-DTA curve of 815 °C CCA

Fig. 5. TGA-DTA thermograms of different biomass ashes at different temperatures

For all biomass ashes, on account of the exothermic reactions among the residual substances, a sharp exothermic peak caused by volatilization of the unburned carbon residuals and other organics in ash was clearly seen between 400 and 500 °C in the DTA curves. Particularly, the contrast of Figs. 5a to 5b, Figs. 5c to 5d, and Figs. 5e to 5f indicated that for the same kind of biomass fuel, the biomass ash formed at 600 °C has a more remarkable weight loss than that of 815 °C ash. With regards to RHA (Figs. 5a and 5b), there was a small endothermic peak within 950 to 1050 °C without any obvious weight loss. Umamaheswaran and Batra (2008) found that the presence of this endothermic peak within 950 to 1050 °C was mainly caused by the melting of amorphous phases and the phase transition of quartz in ash.

For 600 °C RSA (Fig. 5c) and 600 °C CCA (Fig. 5e), the thermal behaviors were basically the same as that of 600 °C RHA (Fig. 5a). In contrast, the 815 °C RSA (Fig. 5d) and 815 °C CCA (Fig. 5f) exhibited continuous weight loss when the temperature exceeded 1000 °C, which was much different from 815 °C RHA (Fig. 5b). Besides, there were no evident subsections of weight loss during the pyrolysis of 815 °C RSA and 815 °C CCA. As can be seen from the DTA curve of 815 °C RSA (Fig. 5d), there was a small endothermic peak near 750 °C due to the melting of KCl dominated mixed salts in ash.

According to previous research (Yao and Xu 2016), the weight loss in a high temperature range could be mainly attributed to the volatilization and the fusion of high-temperature molten materials in biomass ash. Du *et al*. (2014) reported that the weight loss beyond 1000 °C could be caused by the thermal decomposition of some relatively stable K-bearing species (refer to Eq. (1)). Tortosa Masiá *et al*. (2007) suggested that SiO_2 can react with K_2CO_3 which might be from the decomposition of $KHCO_3$ (refer to Eq. (2)). Thus, the continuous weight loss above 1000 °C is partially due to the CO_2 released when K_2CO_3 reacts with SiO_2 (Eq. 3).

$$2K_2SO_4 + 2H_2O \rightarrow 4KOH + 2SO_2(g) \uparrow + O_2(g) \uparrow \quad (1)$$

$$2KHCO_3 \rightarrow K_2CO_3 + H_2O(g) \uparrow + CO_2(g) \uparrow \quad (2)$$

$$K_2CO_3 + xSiO_2 \rightarrow CO_2(g) \uparrow + K_2O \cdot xSiO_2 \ (x = 1, 2, 4) \quad (3)$$

In addition, the DTA curve in Fig. 5f shows that unlike other biomass ashes, there was an endothermic peak around 650 °C, and this endothermic peak was mainly due to the melting of KCl because CCA contains a large amount of KCl in the form of sylvite. Other studies (Nielsen *et al*. 2000; Lin *et al*. 2003) suggest that the intense volatilization of alkali chlorides mainly occurs between 750 and 950 °C.

Influence of Ashing Conditions on Agglomeration Properties of the Ash

To fully understand the influence of ashing temperature and time of exposure on the ash content of biomass as well as on the ash agglomeration properties, those prepared biomass fuels with the same weights were put into a crucible, kept at 600 °C for 2 h or 4 h and at 815 °C for 2 h, 4 h, or 6 h in a muffle furnace. The ash content of biomass under various ashing conditions is listed in Table 5. The surface morphologies of RHA, RSA, and CCA formed under different ashing conditions are presented in Figs. 6 through 8.

Table 5. Ash Content of Different Biomass under Different Ashing Conditions

Ashing Conditions	Ash content (wt.%)		
	RH	RS	CC
600 °C, 2 h	26.34	21.81	22.75
600 °C, 4 h	18.24	17.57	9.51
815 °C, 2 h	20.16	14.89	18.99
815 °C, 4 h	17.82	12.04	7.94
815 °C, 6 h	10.05	8.82	6.83

As shown in Table 5, when the ashing temperature was constant, the ash content of biomass decreased with increased burning time, and this result also indicated that a longer burning time made it easier for the inorganic compounds in biomass to volatilize. When the time of burning and other ashing conditions were constant, the ash content of biomass also decreased with increasing ashing temperature.

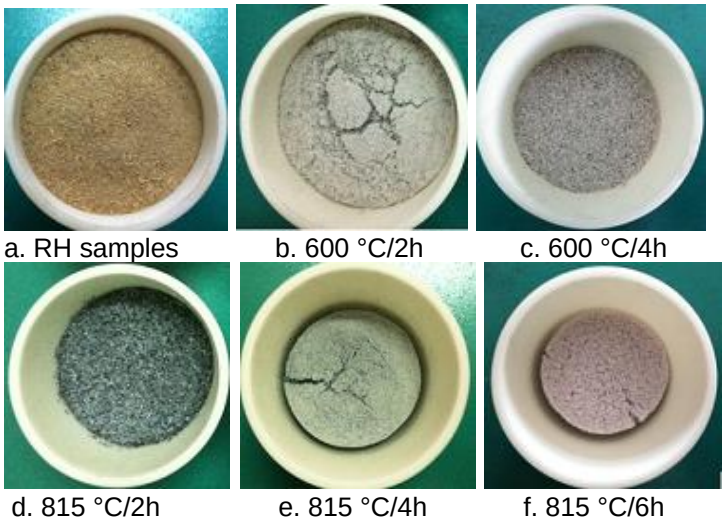

Fig. 6. Apparent morphologies of RH samples and RHA from various ashing conditions

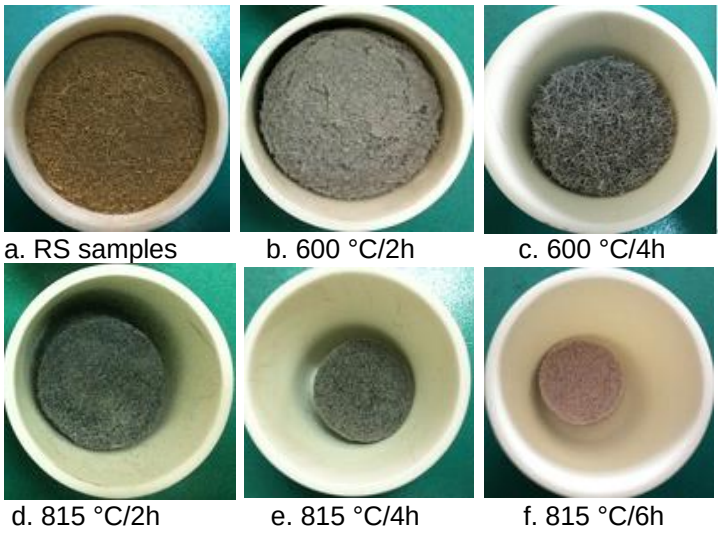

Fig. 7. Apparent morphologies of RS samples and RSA from various ashing conditions

Figures 6a, 7a, and 8a show the pictures of these prepared biomass samples. As shown in Figs. 6b, 7b, and 8b, there were some unburnt compounds in biomass ash because 2 h is probably not enough time for biomass fuels to burn sufficiently, and the color of 600 °C/2h biomass ashes was dark grey. The contrast of Figs. 6d to 6e as well as Figs. 7d to 7e indicated that the number of black particles decreased with the increased burning time, and the surface structures of RHA and RSA become more compact. As can be observed in Fig. 8, the agglomeration degree of 815 °C CCA was more severe than that of 600 °C CCA, which further indicated that the agglomeration degree increased with the increased ashing temperature. In addition, as shown Figs. 6f, 7f, and 8f, the biomass fuels almost burned out under the ashing temperature of 815 °C for 6 h.

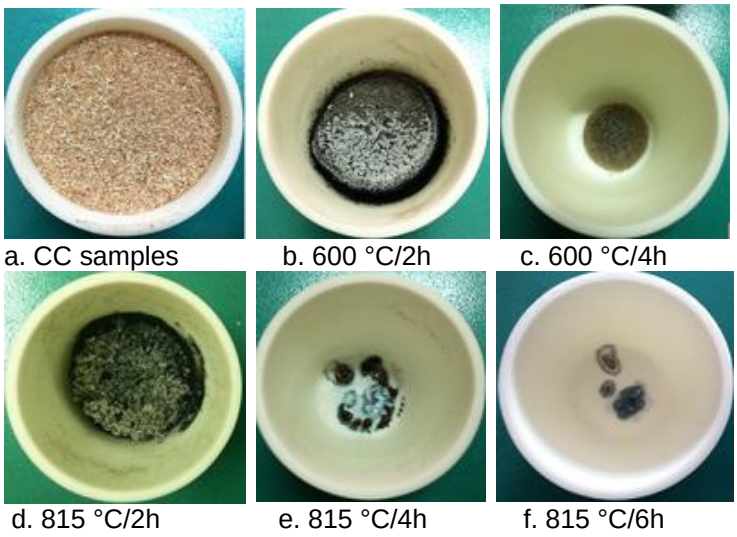

Fig. 8. Apparent morphologies of CC samples and CCA from various ashing conditions

As shown in Figs. 6 through 8, when the ashing temperature was 600 °C, there were almost no black particles in the biomass ash. The colors of biomass ash turned light grey with the increased burning time. Furthermore, whatever the time of burning, there were no black carbon particles observed on the surface of 600 °C biomass ashes, which is in good accordance with the formation mechanism of black particles in RHA (Krishnarao *et al*. 2001). Previous reports (Niu *et al*. 2010a; Du *et al*. 2014) suggested that K_2O starts to decompose at 620 °C, and the released potassium could help these particles containing rich SiO_2 to melt gradually. Hence, after that, parts of the carbon particles were wrapped by the molten SiO_2, which prevented their exposure to air, so they were eliminated by oxidation. Therefore, with regards to 600 °C ashes, the temperature of 600 °C is too low to form black carbon particles.

Slagging and Fouling Characteristics of Biomass Ash

The slagging and fouling characteristics of biomass ash are closely related to the chemical reactions of mineral matters in biomass fuels during the thermo-chemical conversion process. So far, the researchers have put forward several slagging and fouling indices to predict the ash behavior during coal combustion process, but previous studies (Pronobis 2005; Teixeira *et al*. 2012) reported that there is a lack of specific indices for evaluation of slagging and fouling tendency during biomass combustion process. Hence, in this study, the slagging and fouling tendency of biomass ash was evaluated according to the empirical indices for predicting the coal ash behavior during coal combustion.

Analysis of the data in Table 3 showed that the vaporization of alkali metals (mainly including potassium and sodium) can be increased by increasing ashing temperature. To compare the slagging and fouling characteristics of different biomass ashes, the chemical composition of biomass ash formed at 600 °C according to ASTM E1755-01 (2015) was used as a reference.

The formulas for determination of slagging and fouling indices of biomass ash can be described as follows:

The alkali index (*AI*) is defined as the percentage of alkali metal (K_2O + Na_2O) in biomass ash. The index $R_{b/a}$ is defined as the base (Fe_2O_3, CaO, MgO, K_2O, Na_2O) to acid (SiO_2, TiO_2, Al_2O_3) ratio shown in Eq. 4 (Teixeira *et al*. 2012), and this ratio is a mass

ratio. Besides, the formulas of these indices that indicate the ash slagging and fouling tendency were also presented in the following Eqs. 5 to 8 (Pronobis 2005; Xiao *et al*. 2011). In this study, the index *G* is defined as silica ratio (Eq. 5). The index *S/A* is defined as silica-alumina (Eq. 6). H_w is defined as the slagging/fouling index (Eqs. 7 and 8).

$$R_{b/a} = (Fe_2O_3 + CaO + MgO + K_2O + Na_2O) / (SiO_2 + TiO_2 + Al_2O_3) \quad (4)$$

$$G = (SiO_2 \times 100) / (SiO_2 + Fe_2O_3 + CaO + MgO) \quad (5)$$

$$S/A = SiO_2 / Al_2O_3 \quad (6)$$

$$H_w = R_{b/a} \times Na_2O, \text{ as } Fe_2O_3 / (CaO + MgO) > 1 \quad (7)$$

$$H_w = Na_2O, \text{ as } Fe_2O_3 / (CaO + MgO) < 1 \text{ and } CaO + MgO > 2 \quad (8)$$

The results of slagging and fouling indices of different biomass ashes are illustrated in Table 6. The 600 °C RHA contained less alkali metals content, and it fell within the range of "probable slagging and fouling". The 600 °C RSA contained relatively large amounts of alkali metals, falling in the "certain slagging and fouling" range. With regards to the 600 °C CCA, it contained the highest content of alkali metals among these three kinds of biomass ashes. Thus, the slagging propensity of CCA was within the range of "serious slagging and fouling".

Table 6. Results of Slagging and Fouling Indices of Different Biomass Ashes

Biomass Ashes	Decision Indices				
	AI	$R_{b/a}$	*G*	*S/A*	H_w
RHA	2.25	0.047	97.7	259.0	0.39
Slagging and fouling tendency of RHA	Probable	Slight	Slight	Serious	Medium
RSA	14.39	0.30	91.1	284.3	0.93
Slagging and fouling tendency of RSA	Certain	Slight	Slight	Serious	Medium
CCA	33.73	1.30	73.91	11.57	6.18
Slagging and fouling tendency of CCA	Serious	Serious	Medium	Serious	Serious

AI, alkali index; $R_{b/a}$, base-to-acid ratio; *G*, silica ratio; *S/A*, SiO_2 / Al_2O_3; H_w, fouling index.

The $R_{b/a}$ values of RHA and RSA were both smaller than 0.7, and their slagging propensity was slight. This value of CCA was much greater than 0.7, indicating its slagging propensity was serious. The values of *G* for both RHA and RSA were greater than 78.8, and their slagging propensities were slight. The *G* value of CCA was exactly between 66.1 and 78.8, which was in the range of "medium slagging and fouling"; thus the slagging propensity of CCA was medium. The *S/A* values for all the 600 °C ashes were much greater than 2.65, indicating that the slagging propensities of these three biomass ashes were all serious. As for the H_w index, the values of RHA and RSA were smaller than 3, and their slagging and fouling tendencies were medium. The H_w value of CCA was greater than 6, and the slagging propensity was serious.

Based on the above analyses, the slagging and fouling tendency of biomass ash was slightly different with various decision indices, and all biomass ash samples studied in this paper can cause slagging and fouling problems at different levels during the thermo-chemical conversion of biomass fuels.

CONCLUSIONS

1. To fully comprehend the effects of ashing temperature on ash fouling and slagging characteristics during the biomass combustion process, three fuels including rice husk, rice straw, and corn cobs were chosen for this study. Their ashes generated at 600 °C and 815 °C were characterized.
2. Ashing temperatures exerted remarkable influences on ash composition, particle size distribution, ash morphology, fusibility, and thermal analysis. The elevated ashing temperature resulted in the expansion of ash particles and the volatilization of alkali metals in the form of inorganic salts. Based on the XRF results, the systematic slagging/fouling indices were used to study the effects of ashing temperature on the ash fouling and slagging propensities.
3. The slagging and fouling propensity of biomass ash was aggravated by high ashing temperatures. Ash fusion points rose at elevated ashing temperatures, while the ash content decreased. Through thermal properties analysis, a four-step mechanism of weight loss due to volatilization and decomposition was identified. All ashes studied in this paper can result in slagging/fouling problems at different levels.

ACKNOWLEDGMENTS

The authors are grateful for the financial support of Rural Energy Comprehensive Construction Found of the Ministry of Agriculture of China (Grant. No. 2015-36).

REFERENCES CITED

Aho, M., and Silvennoinen, J. (2004). "Preventing chlorine deposition on heat transfer surfaces with aluminium-silicon rich biomass residue and additive," *Fuel* 83(10), 1299-1305. DOI: 10.1016/j.fuel.2004.01.011

ASTM E1755-01 (2015). "Standard test method for ash in biomass," ASTM International, West Conshohocken, USA.

ASTM/E776-87R04 standard (2015). "Standard test method for determination of forms of chlorine in refuse-derived fuel," ASTM International, West Conshohocken, USA.

Ban, C. C., and Ramli, M. (2011). "The implementation of wood waste ash as a partial cement replacement material in the production of structural grade concrete and mortar: An overview," *Resources Conservation and Recycling* 55(7), 669-685. DOI: 10.1016/j.resconrec.2011.02.002

Batra, V. S., Urbonaite, S., and Svensson, G. (2008). "Characterization of unburned carbon in bagasse fly ash," *Fuel* 87(13-14), 2972-2976. DOI: 10.1016/j.fuel.2008.04.010

Brown, R. C., Liu, Q., and Norton, G. (2000). "Catalytic effects observed during the co-gasification of coal and switchgrass," *Biomass Bioenergy* 18(6), 499-506. DOI: 10.1016/S0961-9534(00)00012-X

Demirbas, A. (2002). "Desulfurization of coal using biomass ash," *Energy Sources* 24(12), 1099-1105. DOI: 10.1080/00908310290087021

Du, S. L., Yang, H. P., Qian, K. Z., Wang, X. H., and Chen, H. P. (2014). "Fusion and

transformation properties of the inorganic components in biomass ash," *Fuel* 117, 1281-1287. DOI: 10.1016/j.fuel.2013.07.085

Fang, X., and Jia, L. (2012). "Experimental study on ash fusion characteristics of biomass," *Bioresource Technology* 104, 769-774. DOI: 10.1016/j.biortech.2011.11.055

GB/T212 (2008). "Chinese National Bureau of Standards for coal ash preparation," General Administration of Quality Supervision, Inspection and Quarantine of the People's Republic of China, Beijing.

GB/T219 (2008). "Chinese National Bureau of Standards for determination of fusibility of coal ash," General Administration of Quality Supervision, Inspection and Quarantine of the People's Republic of China, Beijing.

Iliuta, I., Leclerc, A., and Larachi, F. (2010). "Allothermal steam gasification of biomass in cyclic multi-compartment bubbling fluidized-bed gasifier/combustor – New reactor concept," *Bioresource Technology* 101(9), 3194-3208. DOI: 10.1016/j.biortech.2009.12.023

Knudsen, J. N., Jensen, P. A., and Dam-ohansen, K. (2004). "Transformation and release to the gas phase of Cl, K, and S during combustion of annual biomass," *Energy Fuels* 18(5), 1385-1399. DOI: 10.1021/ef049944q

Krishnarao, R. V., Subrahmanyam, J., and Kumar, T. J. (2001). "Studies on the formation of black particles in rice husk silica ash," *Journal of the European Ceramic Society* 21(1), 99-104. DOI: 10.1016/S0955-2219(00)00170-9

Liao, S. W., Lin, C. I., and Wang, L. H. (2011). "Kinetic study on lead (II) ion removal by adsorption onto peanut hull ash," *Journal of the Taiwan Institute of Chemical Engineers* 42(1), 166-172. DOI: 10.1016/j.jtice.2010.04.009

Lin, W. G., Dam-Johansen, K., and Frandsen, F. J. (2003). "Agglomeration in bio-fuel fired fluidized bed combustors," *Chemical Engineering Journal* 96(1-3), 171-185. DOI: 10.1016/j.cej.2003.08.008

Loffler, G., Wargadalam, V. J., and Winter, F. (2002). "Catalytic effect of biomass on CO, CH_4 and HCN oxidation under fluidized bed combustor conditions," *Fuel* 81(6), 711-717. DOI: 10.1016/S0016-2361(01)00203-4

Nielsen, H. P., Baxter, L. L., Sclippab, G., Morey, C., Frandsen, F. J., and Dam-Johansen, K. (2000). "Deposition of potassium salts on heat transfer surfaces in straw-fired boilers: A pilot-scale study," *Fuel* 79(2), 131-139. DOI: 10.1016/S0016-2361(99)00090-3

Niu, Y. Q., Tan, H. Z., Wang, X. B., Liu, Z. N., Liu, H. Y., Liu, Y., and Xu, T. M. (2010a). "Study on fusion characteristics of biomass ash," *Bioresource Technology* 101(23), 9373-9381. DOI: 10.1016/j.fuel.2015.06.010

Niu, Y. Q., Tan, H. Z., Ma, L., Mohamed, P., Liu, Z. N., Liu, Y., Wang, X. B., Liu, H. Y., and Xu, T. M. (2010b). "Slagging characteristics on the superheaters of a 12 MW biomass-fired boiler," *Energy Fuels* 24(9), 5222-5227. DOI: 10.1021/ef1008055

Niu, Y. Q., Du, W. Z., Tan, H. Z., Xu, W. G., Liu, Y. Y., Xiong, Y. Y., and Hui, S. E. (2013). "Further study on biomass ash characteristics at elevated ashing temperatures: The evolution of K, Cl, S and the ash fusion characteristics," *Bioresource Technology* 129, 642-645. DOI: 10.1016/j.biortech.2012.12.065

Niu, Y. Q., Tan, H. Z., and Hui, S. E. (2016). "Ash-related issues during biomass combustion: Alkali-induced slagging, silicate melt-induced slagging (ash fusion), agglomeration, corrosion, ash utilization, and related countermeasures," *Progress in Energy and Combustion Science* 52, 1-61. DOI: 10.1016/j.pecs.2015.09.003

Ogundiran, M. B., Babayemi, J. O., and Nzeribe, C. G. (2011). "Determination of metal

content and an assessment of the potential use of waste cashew nut ash (CNSA) as a source for potash production," *BioResources* 6(1), 529-536. DOI: 10.15376/biores.6.1.529-536

Öhman, M., Nordin, A., Skrifvars, B. J., Backman, R., and Hupa, M. (2000). "Bed agglomeration characteristics during fluidized bed combustion of biomass fuels," *Energy Fuels* 14(1), 169-178. DOI: 10.1021/ef990107b

Pronobis, M. (2005). "Evaluation of the influence of biomass co-combustion on boiler furnace slagging by means of fusibility correlations," *Biomass Bioenergy* 28(4), 375-383. DOI: 10.1016/j.biombioe.2004.11.003

Quaranta, N., Unsen, M., Lopez, H., Giansiracusa, C., Roether, J. A., and Boccaccini, A. R. (2011). "Ash from sunflower husk as raw material for ceramic products," *Ceramics International* 37(1), 377-385. DOI: 10.1016/j.ceramint.2010.09.015

Scala, F., and Chirone, R. (2008). "An SEM/EDX study of bed agglomerates formed during fluidized bed combustion of three biomass fuels," *Biomass Bioenergy* 32(3), 252-266. DOI: 10.1016/j.biombioe.2007.09.009

Sheth, P. N., and Babu, B. V. (2009). "Experimental studies on producer gas generation from wood waste in a downdraft biomass gasifier," *Bioresource Technology* 100(12), 3127-3133. DOI: 10.1016/j.biortech.2009.01.024

Skrifvars, B. J., Lauren, T., Hupa, M., Korbee, R., and Ljung, P. (2004). "Ash behaviour in a pulverized wood fired boiler – A case study," *Fuel* 83(10), 1371-1379. DOI: 10.1016/j.fuel.2004.01.008

Song, H. W., Guo, M. C., and Wang, X. (2003). "The slagging and fouling characteristics of biomass ashes during combustion," *Energy Conservation and Environment Protection* 9, 29-31.

Sun, S. Z., Tian, H. M., Zhao, Y. J., Sun, R., and Zhou, H. (2010). "Experimental and numerical study of biomass flash pyrolysis in an entrained flow reactor," *Bioresource Technology* 101(10), 3678-3684. DOI: 10.1016/j.biortech.2009.12.092

Szemmelveisz, K., Szucs, I., Palotas, A. B., Winkler, L., and Eddings, E. G. (2009). "Examination of the combustion conditions of herbaceous biomass," *Fuel Processing Technology* 90(6), 839-847. DOI: 10.1016/j.fuproc.2009.03.001

Teixeira, P., Lopes, H., Gulyurtlu, I., Lapa, N., and Abelha, P. (2012). "Evaluation of slagging and fouling tendency during biomass co-firing with coal in a fluidized bed," *Biomass Bioenergy* 39(SI), 192-203. DOI: 10.1016/j.biombioe.2012.01.010

Terzioglu, P., Yucel, S., Rababah, T. M., and Ozcimen, D. (2013). "Characterization of wheat hull and wheat hull ash as a potential source of SiO_2," *BioResources* 8(3), 4406-4420. DOI: 10.15376/biores.8.3.4406-4420

Thy, P., Jenkins, B. M., Grundvig, S., Shiraki, R., and Lesher, C. E. (2006). "High temperature elemental losses and mineralogical changes in common biomass ashes," *Fuel* 85(5), 783-795. DOI: 10.1016/j.fuel.2005.08.020

Tortosa Masiá, A. A., Buhre, B. J. P., Gupta, R. P., and Wall, T. F. (2007). "Characterising ash of biomass and waste," *Fuel Processing Technology* 88(11), 1071-1081. DOI: 10.1016/j.fuproc.2007.06.011

Thompson, D. N., Shaw, P. G., and Lacey, J. A. (2003). "Post-harvest processing methods for reduction of silica and alkali metals in wheat straw," *Applied Biochemistry and Biotechnology* 105, 205-218. DOI: 10.1385/ABAB:105:1-3:205

Umamaheswaran, K., and Batra, V. S. (2008). "Physio-chemical characterization of India biomass ashes," *Fuel* 87(6), 628-638. DOI: 10.1016/j.fuel.2007.05.045

Wang, S., Jiang, X. M., Han, X. X., and Wang, H. (2008). "Fusion characteristic study on seaweed biomass ash," *Energy Fuels* 22(4), 2229-2235. DOI: 10.1021/ef800128k

Wei, L. H., Ma, T. T., Li, R. D., Yang, T. H., Li, Y. J., and Wen, L. N. (2014). "Effect of acidic compositions on ash fusion temperatures," *Journal of Fuel Chemistry and Technology* 42 1205-1211. DOI: 10.3969/j.issn.0253-2409.2014.10.008

Wu, P., Yu, C. J., Bai, J. S., Li, L. M., and Huang, F. (2013). "Mechanism study of Chlorine release during biomass pyrolysis," *Proceedings of the Chinese Society for Electrical Engineering* 33(11), 75-81. DOI: 10.13334/j.0258-8013.pcsee.2013.11.012

Xiao, R. R., Chen, X. L., Wang, F. C., and Yu, G. S. (2011). "The physicochemical properties of different biomass ashes at different ashing temperature," *Renewable Energy* 36(1), 244-249. DOI: 10.1016/j.renene.2010.06.027

Xiong, S. J., Burvall, J., Orberg, H., Kalen, G., Thyrel, M., Ohman, M., and Bostrom, D. (2008). "Slagging characteristics during combustion of corn stovers with and without kaolin and calcite," *Energy Fuels* 22(5), 3465-3470. DOI: 10.1021/ef700718j

Yao, X. W., and Xu, K. L. (2016). "Comparative study of characterization and utilization of corncob ashes from gasification process and combustion process," *Construction and Building Materials* 119, 215-222. DOI: 10.1016/j.conbuildmat.2016.04.077

Yao, X. W., Xu, K. L., and Li, Y. (2016). "Physicochemical properties and possible applications of waste corncob fly ash from biomass gasification industries of China," *BioResources* 11(2), 3783-3798. DOI: 10.15376/biores.11.2.3783-3798

Article submitted: November 7, 2016; Peer review completed: December 29, 2016; Revised version received and accepted: January 2, 2017; Published: January 17, 2017.
DOI: 10.15376/biores.12.1.1593-1610